

# POPULATION OF THE SCATTERED KUIPER BELT<sup>1</sup>

Chadwick A. Trujillo

Institute for Astronomy, 2680 Woodlawn Drive, Honolulu, HI 96822  
chad@ifa.hawaii.edu

David C. Jewitt

Institute for Astronomy, 2680 Woodlawn Drive, Honolulu, HI 96822  
jewitt@ifa.hawaii.edu

and

Jane X. Luu

Leiden Observatory, PO Box 9513, 2300 RA Leiden, The Netherlands  
luu@strw.leidenuniv.nl

Received \_\_\_\_\_; accepted \_\_\_\_\_

---

<sup>1</sup>Based on observations collected at Canada-France-Hawaii Telescope, which is operated by the National Research Council of Canada, the Centre National de la Recherche Scientifique de France, and the University of Hawaii.

## ABSTRACT

We present the discovery of three new Scattered Kuiper Belt Objects (SKBOs) from a wide-field survey of the ecliptic. This continuing survey has to date covered 20.2 square degrees to a limiting red magnitude of 23.6. We combine the data from this new survey with an existing survey conducted at the University of Hawaii 2.2m telescope to constrain the number and mass of the SKBOs. The SKBOs are characterized by large eccentricities, perihelia near 35 AU, and semi-major axes  $> 50$  AU. Using a maximum-likelihood model, we estimate the total number of SKBOs larger than 100 km in diameter to be  $N = (3.1_{-1.3}^{+1.9}) \times 10^4$  ( $1\sigma$ ) and the total mass of SKBOs to be  $M \sim 0.05M_{\oplus}$ , demonstrating that the SKBOs are similar in number and mass to the Kuiper Belt inside 50 AU.

*Subject headings:* comets: general — Kuiper Belt, Oort Cloud — solar system: formation

## 1. Introduction

The outer solar system is richly populated by small bodies in a thick trans-Neptunian ring known as the Kuiper Belt (Jewitt et al. 1996). It is widely believed that the Kuiper Belt Objects (KBOs) are remnant planetesimals from the formation era of the solar system and are composed of the oldest, least-modified materials in our solar system (Jewitt 1999). KBOs may also supply the short-period comets (Fernández and Ip 1983; and Duncan et al. 1988). The orbits of KBOs are not randomly distributed within the Belt but can be grouped into three classes. The Classical KBOs constitute about 2/3 of the known objects and display modest eccentricities ( $e \sim 0.1$ ) and semi-major axes ( $41 \text{ AU} < a < 46 \text{ AU}$ ) that guarantee a large separation from Neptune at all times. The Resonant KBOs, which comprise most of the remaining known objects, are trapped in mean-motion resonances with Neptune, principally the 3:2 resonance at 39.4 AU. In 1996, we discovered the first example of a third dynamical class, the Scattered KBOs (SKBOs): 1996TL<sub>66</sub> occupies a large ( $a \sim 85 \text{ AU}$ ), highly eccentric ( $e \sim 0.6$ ), and inclined ( $i \sim 25^\circ$ ) orbit (Luu et al. 1997). It is the defining member of the SKBOs, characterized by large eccentricities and perihelia near 35 AU (Duncan and Levison 1997). The SKBOs are thought to originate from Neptune scattering, as evidenced by the fact that all SKBOs found to date have perihelia in a small range near Neptune ( $34 \text{ AU} < q < 36 \text{ AU}$ ).

In this letter we report preliminary results from a new survey of the Kuiper Belt undertaken at the Canada-France-Hawaii Telescope (CFHT) using a large format Charge-Coupled Device (CCD). This survey has yielded 3 new SKBOs. Combined with published results from an earlier survey (Jewitt et al. 1998) and with dynamical models (Duncan and Levison 1997), we obtain new estimates of the population statistics of the SKBOs. The main classes of KBOs appear in Figure 1, a plan view of the outer solar system.

## 2. Survey Data

Observations were made with the 3.6m CFHT and 12288 x 8192 pixel Mosaic CCD (Cuillandre et al., in preparation). Ecliptic fields were imaged within 1.5 hours of opposition to enhance the apparent sky-plane speed difference between the distant KBOs ( $\sim 3$  arc sec/hr) and foreground main-belt asteroids ( $\gtrsim 25$  arc sec/hr). Parameters of the CFHT survey are summarized in Table 1, where they are compared with parameters of the survey earlier used to identify 1996TL<sub>66</sub> (Luu et al. 1997 and Jewitt et al. 1998). We include both surveys in our analysis of the SKBO population.

Artificial moving objects were added to the data to quantify the sensitivity of the moving object detection procedure (Trujillo and Jewitt 1998). The seeing in the survey varied from 0.7 arc sec to 1.1 arc sec (FWHM). Accordingly, we analysed the data in 3 groups based on the seeing. Artificial moving objects were added to bias-subtracted twilight sky-flattened images, with profiles matched to the characteristic point-spread function for each image group. These images were then passed through the data analysis pipeline. The detection efficiency was found to be uniform with respect to sky-plane speed in the 1 – 10 arc sec/hr range, with efficiency variations due only to object brightness.

The seeing-corrected efficiency function was fitted with a hyperbolic tangent profile for use in the maximum-likelihood SKBO orbital simulation described in Section 3:

$$\varepsilon = \frac{\varepsilon_{\max}}{2} \left( \tanh \left( \frac{m_{R50} - m_R}{\sigma} \right) + 1 \right), \quad (1)$$

where  $0 < \varepsilon < 1$  is the efficiency at detecting objects of red magnitude  $m_R$ ,  $\varepsilon_{\max} = 0.83$  is the maximum efficiency,  $m_{R50} = 23.6$  is the magnitude at which  $\varepsilon = \varepsilon_{\max}/2$ , and  $\sigma = 0.4$  magnitudes is the characteristic range over which the efficiency drops from  $\varepsilon_{\max}$  to zero.

The orbital parameters of the 4 established SKBOs are listed in Table 2. It should be noted that the 3 most recent KBOs have been observed for a timebase of about 3 months,

so their fitted orbits are subject to revision. However, the 4 year orbit of 1996TL<sub>66</sub> has changed very little since its initial announcement with a 3 month arc ( $a = 85.754$ ,  $e = 0.594$ ,  $i = 23.9$ ,  $\omega = 187.7$ ,  $\Omega = 217.8$ ,  $M = 357.3$ , and epoch 1996 Nov 13; Marsden 1997). A plot of eccentricity versus semi-major axis appears in Figure 2, showing the dynamical distinction of SKBOs from the other KBOs. All SKBOs have perihelia  $34 \text{ AU} < q < 36 \text{ AU}$ . To avoid confusion with Classical and Resonant KBOs also having perihelia in this range, we concentrate on the SKBOs with semi-major axes  $a > 50 \text{ AU}$ . In so doing, we guarantee that our estimates provide a solid lower bound to the true population of SKBOs.

### 3. Population Estimates

The number of SKBOs can be crudely estimated by simple extrapolation from the discovered objects. The faintest SKBO in our sample, 1999CY<sub>118</sub>, was bright enough for detection only during the 0.24% of its  $\sim 1000$  year orbit spent near perihelion. Our 20.2 square degrees of ecliptic observations represent  $\sim 1/500$ th of the total  $\pm 15^\circ$  thick ecliptic, roughly the thickness of the Kuiper Belt (Jewitt et al. 1996). Thus, we crudely infer the population of SKBOs to be of order  $500/2.4 \times 10^{-3} \sim 2 \times 10^5$ . To more accurately quantify the population, we use a maximum-likelihood method to simulate the observational biases of our survey.

Our discovery of 4 SKBOs with the CFHT and UH telescopes provides the data for the maximum-likelihood simulation. We assess the intrinsic population of SKBOs by the following procedure (c.f. Trujillo 2000): (1) create a large number ( $\sim 10^8$ ) of artificial SKBO orbits drawn from an assumed distribution; (2) determine the ecliptic latitude, longitude, and sky-plane velocity of each artificial object, using the equations of Sykes and Moynihan (1996; a sign error was found in equation 2 of their text and corrected before use), and compute the object’s brightness using the  $H$ ,  $G$  formalism of Bowell et al. (1989),

assuming an albedo of 0.04; (3) determine the detectability of each artificial object based on the detection efficiency and sky-area imaged in the two surveys; (4) create a histogram of “detected” artificial objects in  $a-e-i$ -radius space, with a bin size sufficiently small such that binning effects are negligible; (5) based on this histogram, compute the probability of finding the true, binned, observed distribution of the four SKBOs, assuming Poisson detection statistics; and (6) repeat the preceding steps, varying the total number of objects in the distribution ( $N$ ) and the slope ( $q' = 3, 4$ ) of the differential size distribution to find the model most likely to produce the observations. A full description of the model parameters is found in Table 3.

This model was designed to match the SKBO population inclination distribution, eccentricity distribution, and ecliptic plane surface density as a function of heliocentric distance, as found in the only published SKBO dynamical simulation to date, that of Duncan and Levison (1997). It should be noted that the results of the 4 billion year simulations of Duncan and Levison (1997) were based on only 20 surviving particles, averaged over the last 1 billion years of their simulation for improved statistical accuracy. The total number of objects and the size distribution of objects remained free parameters in our model.

#### 4. Results

The results of the maximum-likelihood simulation appear in Figure 3. Confidence levels were placed by finding the interval over which the integrated probability distribution corresponded to 68.27% and 99.73% of the total, hereafter referred to as  $1\sigma$  and  $3\sigma$  limits, respectively. The total number of SKBOs with radii between 50 km and 1000 km is  $N = (3.1_{-1.3}^{+1.9}) \times 10^4$  ( $1\sigma$ ) in the  $q' = 4$  case, with  $4.0 \times 10^3 < N < 1.1 \times 10^5$   $3\sigma$  limits. The  $q' = 3$  case is similar with  $N = (1.4_{-0.5}^{+1.1}) \times 10^4$  ( $1\sigma$ ), with  $2.0 \times 10^3 < N < 5.3 \times 10^4$   $3\sigma$

limits. The  $q' = 4$  and  $q' = 3$  best fits are equally probable at the  $< 1\sigma$  level, however we prefer the  $q' = 4$  case as recent measurements of the Kuiper Belt support this value (Jewitt et al. 1998, Gladman and Kavelaars 1998, Chiang and Brown, 1999). This population is similar in number to the Kuiper Belt interior to 50 AU, which contains about  $\sim 10^5$  objects (Jewitt et al. 1998). The observation that only a few percent of KBOs are SKBOs is due to the fact that the SKBOs are only visible in magnitude-limited surveys during the small fraction of their orbits when near perihelion. In addition, the high perihelion velocities,  $v$ , of eccentric SKBOs may have implications for erosion in the Kuiper Belt since ejecta mass,  $m_e$ , scales with impact energy,  $E$ , as  $m_e \sim E^2 \sim v^4$  (Fujiwara et al. 1977).

Extrapolating the  $q' = 4$  distribution to the size range  $1 \text{ km} < r < 10 \text{ km}$  yields  $N \sim 4 \times 10^9$  SKBOs in the same size range as the observed cometary nuclei. This is comparable to the  $10^9$  needed for the SKBOs to act as the sole source of the short-period comets (Levison and Duncan 1997).

The total mass  $M$  of objects assuming  $q' = 4$  is

$$M = 2.3 \times 10^{-3} p_R^{3/2} \frac{\rho}{\text{kg m}^{-3}} \log\left(\frac{r_{\max}}{r_{\min}}\right) M_{\oplus}, \quad (2)$$

where red geometric albedo  $p_R = 0.04$ , density  $\rho = 2000 \text{ kg m}^{-3}$ , the largest object  $r_{\max} = 1000 \text{ km}$  (Pluto-sized), and smallest object  $r_{\min} = 50 \text{ km}$  yields  $M \sim 0.05 M_{\oplus}$ , where  $M_{\oplus} = 6 \times 10^{24} \text{ kg}$  is the mass of the earth. This is comparable to the total mass of the Classical and Resonant KBOs ( $0.2 M_{\oplus}$ , Jewitt et al. 1998). If only 1% percent of SKBOs have survived for the age of the solar system (Duncan and Levison 1997), then an initial population of  $10^7$  SKBOs ( $50 \text{ km} < r < 1000 \text{ km}$ ) and a SKBO primordial mass  $\gtrsim 5 M_{\oplus}$  are inferred.

As our observations are concentrated near the ecliptic, we expected most of the discovered objects to have low inclinations. However, of the 4 established SKBOs, 3 have high inclinations ( $i \gtrsim 20^\circ$ ). The possibility of a Gaussian distribution of inclinations

centered at  $i \sim 20^\circ$  was tested, however, the fit was not better than the uniform  $i$  case at the  $\geq 3\sigma$  level. If the SKBOs were distributed as such, the total numbers of SKBOs reported here would be enhanced by a factor  $\sim 2$ . Combining this model-dependent uncertainty, the orbital uncertainties of the 4 SKBOs, and the computed Poisson noise, we estimate that our predictions provide an order-of-magnitude constraint on the population of the SKBOs. As additional SKBOs become evident in our continuing survey and as recovery observations of the SKBOs are secured, we will refine this estimate.

## 5. Summary

We have constrained the SKBO population using surveys undertaken on Mauna Kea with two CCD mosaic cameras on two telescopes. The surveys cover 20.2 square degrees to limiting red magnitude 23.6 and 51.5 square degrees to limiting red magnitude 22.5. We find the following:

(1) The SKBOs exist in numbers comparable to the KBOs. The observations are consistent with a population of  $N = (3.1_{-1.3}^{+1.9}) \times 10^4$  ( $1\sigma$ ) SKBOs in the radius range  $50 \text{ km} < r < 1000 \text{ km}$  with a differential power-law size distribution exponent of  $q' = 4$ .

(2) The SKBO population in the size range of cometary nuclei is large enough to be the source of the short-period comets.

(3) The present mass of the SKBOs is approximately  $0.05M_\oplus$ . When corrected for depletion inferred from dynamical models (Duncan and Levison 1997), the initial mass of SKBOs in the early solar system approached  $5M_\oplus$ .

We are continuing our searches for these unusual objects as it is clear that they play an important role in outer solar system dynamics.



We thank Ken Barton for help at the Canada-France-Hawaii Telescope. This work was supported by a grant to DCJ from NASA.

## REFERENCES

- Bowell, E., Hapke, B., Domingue, D., Lumme, K., Peltoniemi, J., Harris, A. 1989, in Asteroids II, edited by R. Binzel, T. Gehrels, and M. Matthews (University of Arizona, Tucson). p. 524–556
- Chiang, E. I. and Brown, M. E. 1999, *AJ*, 118, 1411
- Cuillandre, J.-C., Starr, B., Isani, S., Luppino, G. A., and Tonry, J., 1999, *PASP*, in preparation
- Duncan, M. J. and Levison, H. F. 1997, *Science*, 276, 1670
- Duncan, M., Quinn, T., Tremaine, S. 1988, *ApJ*, 328, 69
- Fernández, J., A., and Ip, W.-H. 1983, *Icarus*, 54, 377
- Fujiwara, A., Kamimoto, G., and Tsukamoto, A. 1977, *Icarus*, 31, 277
- Gladman B. and Kavelaars, J. J. 1998, *AJ*, 116, 2042
- Jewitt, D. 1999, *Annu. Rev. Earth. Planet. Sci*, 27, 287
- Jewitt, D., Luu, J., and Chen, J. 1996, *AJ*, 112, 1225
- Jewitt, D., Luu, J., and Trujillo, C. 1998, *AJ*, 115, 2125
- Kenyon, S. J. and Luu, J. X. 1999, *AJ*, 118, 1101
- Luu, J., Marsden, B. G., Jewitt, D., Trujillo, C. A., Hergenrother, C. W., Chen, J., and Offutt, W. B. 1997, *Nature*, 387, 573
- Marsden, B. MPEC 1997-B18
- Sykes, M. V. and Moynihan, P. D. 1996, *Icarus*, 124, 399

Trujillo, C. 2000, in press, in *Minor Bodies in the Outer Solar System, 1998* (Springer-Verlag, Heidelberg)

Trujillo, C. and Jewitt, D. 1998, *AJ*, 115, 1680

## 6. Figure Captions

Fig. 1.— A plan view of the outer solar system; the green circle represents the orbit of Jupiter. Kuiper Belt Objects have been color-coded based on their orbital classification. The SKBO orbits are distinct.

Fig. 2.— The KBOs (hollow) and the 4 SKBOs (solid). The 3:2 and 2:1 resonances are shown as dashed lines. The solid lines represent perihelia of  $q = 34$  and  $36$ .

Fig. 3.— Probability that the model matches the observed distribution of SKBOs versus the total number of objects in the model for the  $q' = 4$  size distribution. The maximum likelihood is given by  $N = (3.1_{-1.3}^{+1.9}) \times 10^4$  ( $1\sigma$ ). The dashed lines represent the  $1\sigma$  and  $3\sigma$  limits.

Table 1. Survey Parameters

Quantity	UH 2.2m	CFHT 3.6m
Focal Ratio	f/10	f/4
Instrument	UH 8k Mosaic	CFHT 12k x 8k Mosaic
Plate Scale [arc sec/pixel]	0.135	0.206
Field Area [deg <sup>2</sup> ]	0.09	0.33
Total Area [deg <sup>2</sup> ]	51.5	20.2
$m_{R50}$ <sup>a</sup>	22.5	23.6
$\theta^b$ [arc sec]	0.8–1.0	0.7–1.1
Filter	<i>VR</i> <sup>c</sup>	<i>R</i>
Quantum Efficiency	0.33	0.75
$N_{\text{SKBOs}}^d$	1	3

<sup>a</sup>The red magnitude at which detection efficiency reaches half of the maximum efficiency.

<sup>b</sup>the typical Full Width at Half Maximum of stellar sources for the surveys.

<sup>c</sup>The *VR* filter has a high transmission in the 5000 – 7000 Å range (Figure 1 of Jewitt et al., 1996).

<sup>d</sup>The number of SKBOs detected.

Table 2. The SKBOs\*

	1996TL <sub>66</sub>	1999CV <sub>118</sub>	1999CY <sub>118</sub>	1999CF <sub>119</sub>
Orbital Properties				
$a$ [AU]	85.369	56.532	95.282	115
$e$	0.590	0.387	0.642	0.687
$i$ [deg]	23.9	5.5	25.6	19.7
$\omega$ [deg]	184.5	126.6	21.4	218.1
$\Omega$ [deg]	217.8	305.6	163.1	303.4
$M$ [deg]	359.2	22.5	356.4	354.3
epoch	1999 Aug 10	1999 Mar 23	1999 Mar 23	1999 Mar 23
Discovery Conditions				
date	1996 Oct 09	1999 Feb 10	1999 Feb 10	1999 Feb 11
$R$ [AU]	35.2	39.7	38.6	42.2
$m_R$	20.9	23.0	23.7	23.0
$m_R(1, 1, 0)$	5.3	7.0	7.8	6.7
Diameter [km]	520	240	170	270

Note. —  $a$ ,  $e$ ,  $i$ ,  $\omega$ ,  $\Omega$ , and  $M$  represent the Keplerian orbital elements semi-major axis, eccentricity, inclination, argument of perihelion, longitude of the ascending node, and mean anomaly at the given epoch.  $R$  is the heliocentric distance.  $m_R$  is the red magnitude at discovery.  $m_R(1, 1, 0)$  is red magnitude at zero phase angle, geocentric distance =  $R = 1$  AU, assuming a phase darkening law for dark objects (Bowell, et al. 1989). The diameter is derived assuming a geometric albedo of 4%.

\*Orbital elements from B. Marsden, Minor Planet Center, Harvard-Smithsonian Center for Astrophysics.

Table 3. Model Parameters

Symbol	Value	Distribution	Description
$a$	50 – 200 AU	note <sup>a</sup>	semi-major axis
$e$	0 – 1	uniform	eccentricity
$i$	0 – 35 deg	uniform	inclination
$\omega$	0 – 360 deg	uniform	argument of perihelion
$\Omega$	0 – 360 deg	uniform	longitude of the ascending node
$M$	0 – 360 deg	uniform	mean anomaly
$r$	50 – 1000 km	$n(r)dr \sim r^{-q'} dr$	radius
$q'$	3, 4	—	slope parameter
$p_R$	0.04	—	red albedo
$N$	free	—	total number of objects
$q$	34 – 36 AU	note <sup>b</sup>	perihelion distance

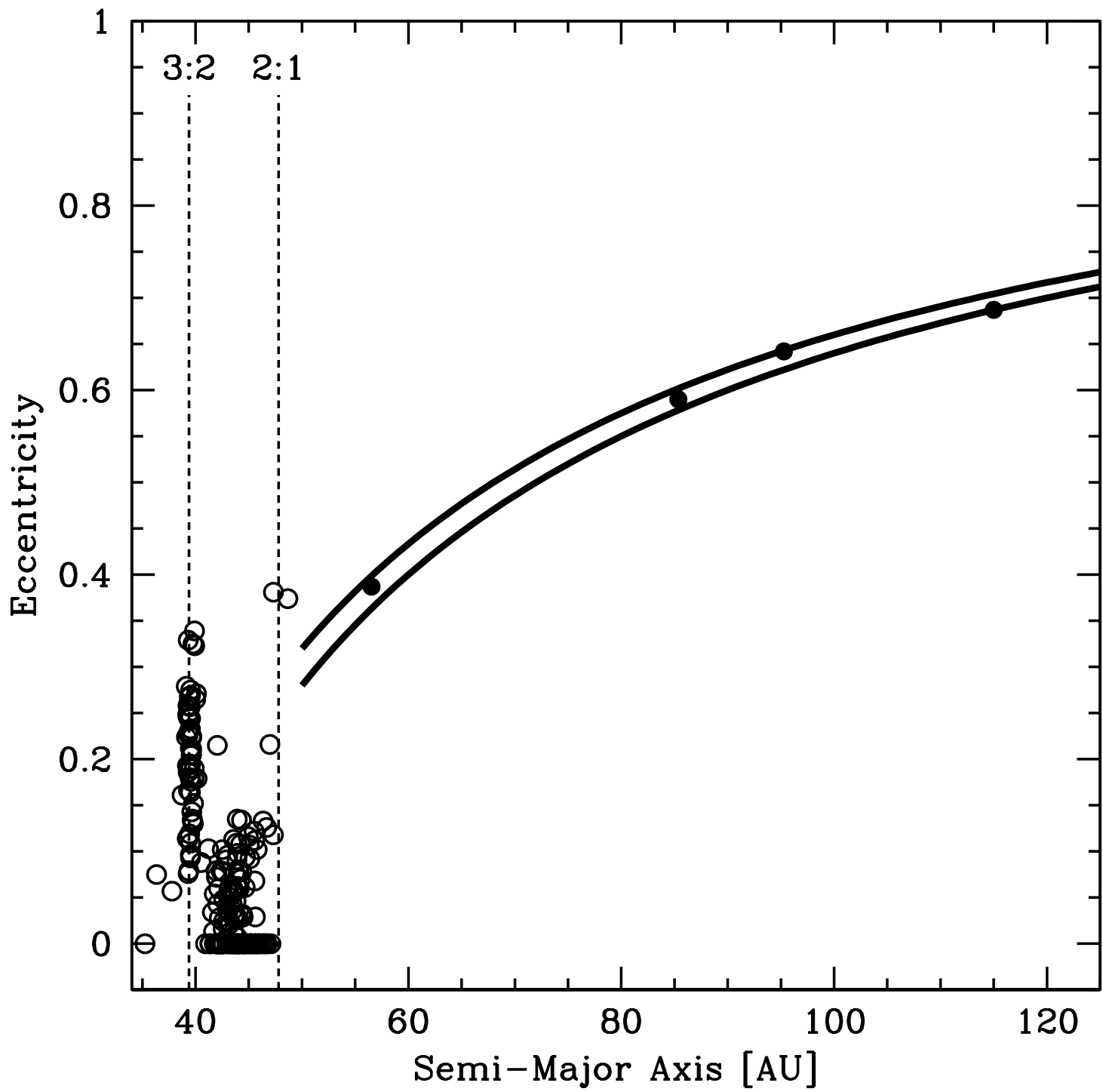
<sup>a</sup>Semi-major axis was chosen such that the surface density of objects versus heliocentric distance follows  $n(R) \sim R^{-p}dR$ , where  $p = 2.5$  (Duncan and Levison 1997).

<sup>b</sup>Perihelion distance was selected by first choosing  $a$  and then limiting  $e$  such that objects were in the 34 to 36 AU range.

This figure "figure1.jpg" is available in "jpg" format from:

<http://arxiv.org/ps/astro-ph/9912428v1>





Probability (Observed = Simulated)

